

Optimization of Poly-Si/SiO_x Passivated Contacts for Crystalline Silicon Bottom Cells Applications

Julci Ditsougou^{1,2,*} , Thibaut Desrues¹ , Anne Kaminski² , and Sébastien Dubois¹ 

¹ Université Grenoble Alpes, CEA, Liten

² Université Grenoble Alpes, CNRS, Université Savoie Mont Blanc, Grenoble INP, CROMA

*Correspondence: Julci Ditsougou, julci.ditsougou@cea.fr

Abstract. In this study we investigate the coupled impacts of poly-Si thickness, dopant activation annealing temperature and hydrogenation on n-TOPCon and p-TOPCon passivated contacts. Their performance is first assessed by Photoconductance Decay (PCD) measurements on symmetrical and asymmetrical cell precursors before being evaluated on cells by I-V characterizations. We show that high-temperature annealing of poly-Si layers is responsible for excessive dopants penetration in the substrate, which can then be limited by the presence of a thicker poly-Si layer. Moreover, these thicker poly-Si layers benefit more from hydrogenation steps, enabling $i-V_{oc}$ of around 720 mV and carrier lifetimes of up to 5 ms on cell precursors. Finally, while increasing the thickness leads to current limitation under AM1.5G (1 Sun) illumination, this limitation is less pronounced under IR illumination. We therefore demonstrate that for tandem applications, the bottom-cell can benefit from a gain in V_{oc} and FF without suffering from a major optical limitation.

Keywords: TOPCon, Passivated Contact, Hydrogenation, Solar Cell, Bottom-Cell, 2T Tandem, Variable Illumination

1. Introduction

High surface passivation and easy interconnection appear to be among the most important factors for integrating a silicon-based cell as a bottom-cell in two terminals (2T) tandem devices. Following the example of passivated contact technologies such as Silicon Heterojunctions (SHJ), Tunnel Oxide Passivated contacts (TOPCon) cell technologies featuring poly-Si/SiO_x structures should be able to perfectly respond to these requirements [1], [2]. In TOPCon devices, the surface passivation is further enhanced by the use of a highly doped poly-Si layer (n^+ or p^+), which creates a field effect offering greater selectivity and by the presence of a tunnel SiO_x, which saturates the dangling bonds at the wafer surface[3]. TOPCon contacts may also offer specific advantages for integration in 2T devices. Here, the presence of intermediate layers at the interface between the sub-cells is usually important. These layers should enable the extraction and recombination of the carriers generated in the top-cell and bottom-cell to ensure the continuity of the current in the device. The mainstream approach consists in the integration of an In-rich TCO (Transparent and Conductive Oxide) layer at the interface between both sub-cells. As poly-Si layers are obtained through high T processes, they are tolerant to post-process annealing which turns to be advantageous when it comes to the optimization of both the optical and electrical properties of alternative intermediate layers, either as a replacement for ITO or in conjunction with it. In addition, when placed on the front side of the bottom-cell, the crystalline nature of the poly-Si layers could also facilitate the deposition

and growth of a second, highly counter-doped crystalline layer for the formation of a tunnel diode (p^{++}/n^{++}) also known as a tunnel recombination junction (TRJ) [3], [4], [5].

Here we focus on a device incorporating poly-Si/SiO_x passivated contacts on both sides, referred to as TOPCon². Our reference process for single-junction applications (depicted in **Figure 1** and fully described in references [6], [7]), mainly consists in a thermal oxidation followed by the formation of poly-Si layers (15 nm thick) doped by Plasma Ion Immersion Implantation (PIII) and high temperature annealing around 875°C. On the one hand, the steps involved in forming the poly-Si layers (i.e., layer deposition, doping and dopant activation annealing) have a strong influence on the surface passivation through the field effect imparted to the contact formed. On the other hand, hydrogenation steps can further optimize the chemical passivation since hydrogen atoms are known to saturate the remaining dangling bonds at the wafer surface [8], [9]. If properly optimized, the two phenomena mentioned above can enable these devices to target implied Open Circuit Voltages ($i-V_{oc}$) > 730 mV [10], making them suitable for integrations in tandem architectures. In this work, with the aim at improving the surface passivation of our device, we investigate the impact on the performances of the passivated contacts formed of i) the poly-Si layer thickness and dopant activation annealing temperature ii) hydrogenation steps. To understand the distinct influences of these parameters on the electron and hole collectors, we first process symmetrical samples with n-TOPCon and p-TOPCon. Both contacts are then combine on asymmetrical cells precursors.

We use Photo Conductance Decay (PCD) measurements to monitor the passivation performances of our samples. The precursors are brought up to cell level on which we carry out two I-V measurements, one under conventional 1 Sun spectrum (AM1.5G spectrum), the second under a filtered spectrum deprived from UV wavelengths to assess the performances for both single junction and tandem applications.

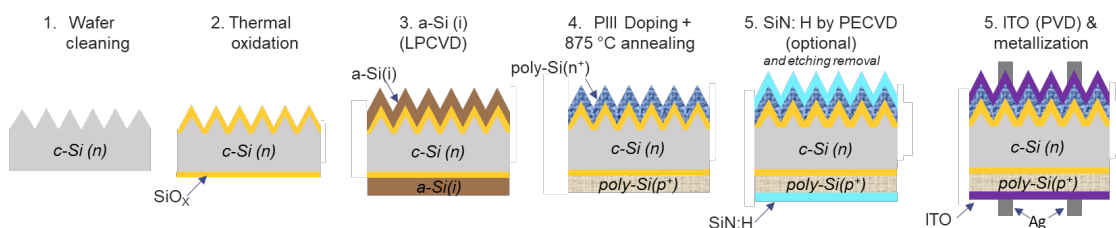


Figure 1: Process flow of TOPCon² devices produced for this study.

2. Experimental details

All the samples in this study were fabricated using M2 (243.36 cm²), n-type, Czochralski (Cz) wafers with a thickness of 160 μm. Three types of samples have been fabricated (**Figure 2**): (i) Symmetrical ones integrating p-TOPCon on both sides, (ii) symmetrical ones integrating n-TOPCon on both sides and (iii) asymmetrical ones integrating n-TOPCon on the textured front surface and p-TOPCon on the polished rear surface. Symmetrical samples with p-TOPCon and n-TOPCon were respectively made on wafers with double side polished and textured surfaces. Symmetrical and asymmetrical cell precursor samples were obtained following the reference process flow described in **Figure 1** without the metallization step.

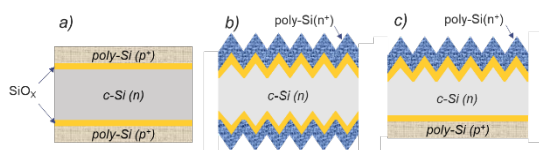


Figure 2: Structure of fabricated (a) p-TOPCon symmetrical samples, (b) n-TOPCon symmetrical samples and (c) asymmetrical cell precursor samples.

After the chemical cleaning, we made a thermal oxidation at 500°C for the formation of a tunnel SiO_x with a thickness around 1.5 nm. We then made the Low Pressure Chemical Vapor deposition (LPCVD) process of intrinsic amorphous silicon a-Si (i) layers. In order to assess the impact of the poly-Si layer thickness, we investigate three (3) LPCVD process durations, resulting in the following poly-Si thicknesses: 15 nm (our reference), 30 nm and 50 nm.

PH₃ was used to dope the a-Si (i) layers. We used B₂H₆ and PH₃ gas precursors depending on the polarity targeted. A high temperature annealing step (the dopant activation annealing) was then performed to finalize the formation of the passivated contacts, allowing the dopants diffusion and activation. The dopant activation annealing also conducts to the transition of a-Si layers in a crystalline poly-Si phase. For all samples polarities and poly-Si thicknesses, we investigated annealing temperatures between 875°C and 950°C. The duration process and the other parameters were kept unchanged.

All samples were capped by a Plasma Enhanced Chemical Vapor Deposited (PECVD) SiN:H layer, for hydrogenation purpose. No additional firing was performed. After deposition, this SiN:H layer was etched off by HF.

Secondly, we also fabricated cells from the non-hydrogenated asymmetrical precursors. For this purpose, the asymmetrical samples after the activation annealing process experienced a chemical cleaning before the deposition by sputtering of an ITO layer and the screen-printing of Ag metallization.

PCD measurements were performed to assess the passivation performances on symmetrical and asymmetrical samples. Electrochemical Capacitance-Voltage (ECV) profiling was also conducted on some samples. For the cells, we performed an IV characterization under AM1.5G illumination and a truncated AM1.5G spectrum (IR). The truncated spectrum was obtained using a high-pass filter cutting around 700 nm to consider only the spectrum received by the silicon cell integrated in a tandem device.

3. Results and discussion

3.1 On the poly-Si thickness and the annealing temperature

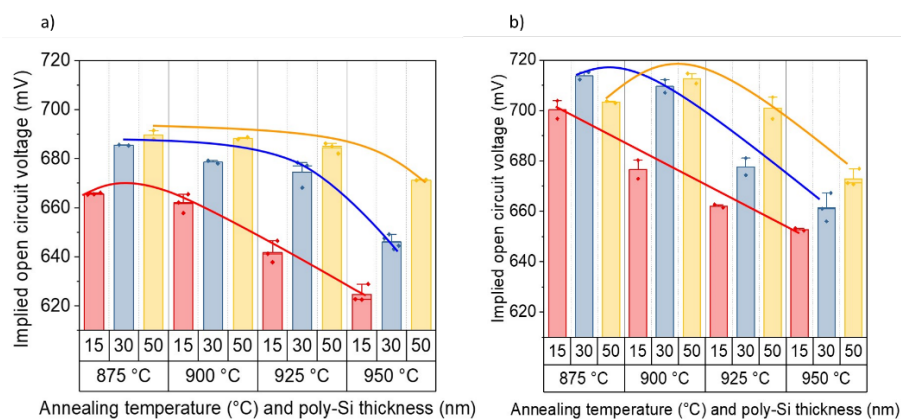


Figure 3: $i-V_{oc}$ values for (a) p-TOPCon and (b) n-TOPCon symmetrical samples for different poly-Si thicknesses and activation annealing temperatures (with corresponding trends lines).

We first investigated the coupled impacts of the poly-Si thickness and the dopant activation annealing temperature on the surface passivation level for p-TOPCon and n-TOPCon. $I-V_{oc}$ values from PCD measurements help us to assess these performances. We depicted the results for our p-TOPCon and n-TOPCon symmetrical samples in **Figure 3**.

For p-TOPCon, we can see that whatever the annealing temperature, the $i-V_{oc}$ values increase with the poly-Si thickness. Furthermore, for a given poly-Si thickness, we can observe that increasing the annealing temperature leads to a decrease in the $i-V_{oc}$ values. 875°C appears as an optimal temperature for all thickness conditions. The highest $i-V_{oc}$ for these symmetrical p-TOPCon samples was of 690 mV, for a 50 nm-thick poly-Si layer annealed at 875°C.

Focusing on the symmetrical n-TOPCon samples, at 875°C an optimum $i-V_{oc}$ value can be found for the 30 nm condition. For temperatures $\geq 900^\circ\text{C}$, the trend is the same as for p-TOPCon structures: an increase in the poly-Si layer thickness leads to an increase in the $i-V_{oc}$ values. Here if there is still an optimal temperature for an efficient passivated contact, it appears to be very sensitive to the poly-Si thickness as shown by the colored trend lines in **Figure 3.b**. The best $i-V_{oc}$ on these symmetrical n-TOPCon samples were obtained on the 30 nm sample annealed at 875°C with 709 mV and the 50 nm sample annealed at 900°C with 713 mV.

To further investigate the poly-Si thickness beneficial impact on $i-V_{oc}$, we compared ECV profiles of symmetrical p-TOPCon samples with 15 nm and 50 nm poly-Si thicknesses for different annealing temperatures. The results are depicted in **Figure 4.a**. We can see that for a fixed poly-Si thickness, increasing annealing temperature leads to a further diffusion of the dopants (holes) in the material (i.e., Si substrate) depth. For example, regarding the sample with a 15 nm poly-Si layer and a 875°C annealing (black square symbols), the active dopant concentration is lower than 10^{16} cm^{-3} after 160 nm. In comparison, for a 950°C annealing (blue downward triangle symbols), we can see an active dopant concentration close to 10^{19} cm^{-3} up to 275 nm in the depth of the structure. Such high dopant concentrations result in increased Auger recombination. This effect can be responsible for the low passivation levels observed with the samples featuring the thinnest poly-Si layers and the highest annealing temperatures. On the other hand, looking at the 50 nm thickness conditions, we can see that for a given annealing temperature we have less dopant diffusion within the Si substrate than for the 15 nm-thick poly-Si samples. To illustrate this trend we compare the 875°C annealing data (black square symbols) for both samples. At 100 nm in the structure depth, the 15 nm poly-Si sample still has an active dopant concentration close to 10^{19} cm^{-3} while the 50 nm poly-Si sample is already well below 10^{16} cm^{-3} . This means that thicker poly-Si layers limit the diffusion of dopants in the Si substrate, lowering the extent of Auger recombination and therefore favoring better passivation levels.

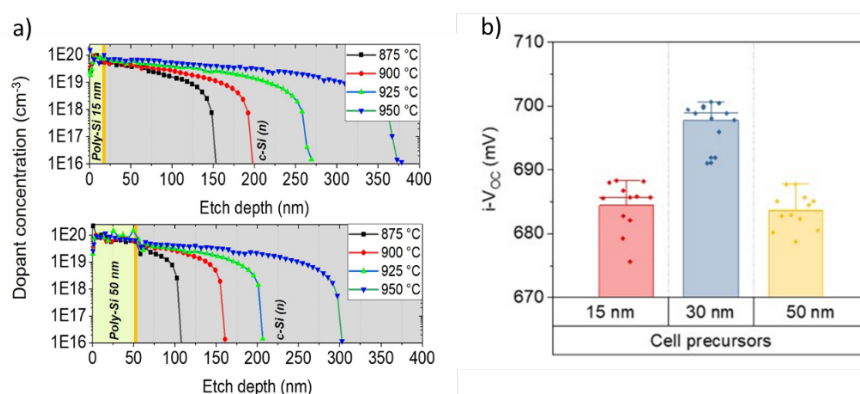


Figure 4: a) Doping profiles with different activation annealing temperatures from ECV measurements of p-TOPCon symmetrical samples with 15 nm (top) and 50 nm (bottom) poly-Si thicknesses. b) Evolution of $i-V_{oc}$ of asymmetrical cell precursor samples with different poly-Si layers thickness. The samples were annealed at 875°C for dopants activation.

Considering that our solar cell process includes a single dopant activation annealing step for both passivated contacts (i.e., p- and n-type), we only considered a dopant activation annealing temperature of 875°C for the cell precursors preparation, since this temperature appears to be a good compromise for both polarities. The $i-V_{oc}$ values for these asymmetrical cell

precursor samples are plotted in **Figure 4.b**. With a view on symmetrical samples results (**Figure 3**), it can be assumed that the precursors with 50 nm poly-Si layers suffer from the low $i-V_{oc}$ observed on the n-TOPCon symmetrical samples. Moreover, the precursors with 15 nm poly-Si layers suffer from the low $i-V_{oc}$ observed on both the p-TOPCon and the n-TOPCon symmetrical samples with the same thickness. We then observe that the best performances are obtained for the precursors having a 30 nm-thick poly-Si layer with $i-V_{oc}$ values around 698 mV. This value represents an improvement of around +13 mV compared to our reference process featuring $i-V_{oc}$ values around 685 mV.

3.2 On the hydrogenation of passivated contacts

Hydrogenation process by SiN:H layer was performed on symmetrical p-TOPCon samples, symmetrical n-TOPCon samples and asymmetrical cell precursors. The hydrogenation process was carried out on symmetrical samples which experienced different dopant activation annealing temperatures. However, even after hydrogenation, the best performances were still obtained with the 875°C annealing conditions for both p-TOPCon and n-TOPCon samples. Here also, we thus limited the study on asymmetrical samples annealed at 875°C as this value was confirmed as the optimum for our process. We compare $i-V_{oc}$ values on p-TOPCon and n-TOPCon symmetrical devices post annealing (P.A.) and after the hydrogenation process and the removal of the SiN: H layer (P.H.). The results are depicted in **Figure 5**.

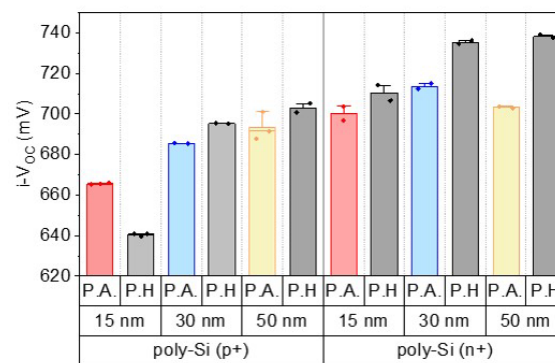


Figure 5: Comparison of $i-V_{oc}$ for symmetrical p-TOPCon (left) and n-TOPCon (right) samples after the activation annealing (P.A.) and after the hydrogenation process through SiN:H deposition and removal (P.H.).

Regarding the symmetrical samples, we can see that thicker poly-Si layers show a better response to hydrogenation. For hydrogenated p-TOPCon symmetrical samples, 30 and 50 nm conditions exhibit $i-V_{oc}$ values of 695 mV and 703 mV, respectively. Moreover, $i-V_{oc}$ values close to 740 mV were obtained on same poly-Si thickness conditions for hydrogenated symmetrical n-TOPCon samples. In the case of 15 nm poly-Si layers, hydrogenation appears to be unproductive or even detrimental. Indeed, we observe a drop in $i-V_{oc}$ values after hydrogenation on symmetrical p-TOPCon devices and a smaller increase compared with the other thickness conditions when looking on symmetrical n-TOPCon devices. As observed with ECV measurements, thinner poly-Si layers were much more prone to high penetration of dopants within the substrate. An hypothesis could be that higher dopant penetration could also lead to deterioration of the SiO_x tunnel oxide [11]. Such a deterioration could operate differently between p- and n-TOPCon structures due to the differences in the diffusion behaviors of boron and phosphorus atoms. Therefore, while we observe a slight improvement for 15 nm n-TOPCon devices, it is likely that a major and irreversible deterioration of the oxide occurs on the 15 nm samples for p-TOPCon, thus preventing any curing effect during hydrogenation.

The results obtained for asymmetrical cell precursors are presented in **Figure 6**. Here also we can observe that thicker poly-Si layers perform better after the hydrogenation step. As

they exhibit the coupling effect of both TOPCon polarities, we can assess that the drop observed for the 15 nm condition is due to the one observed on the 15 nm p-TOPCon symmetrical samples (**Figure 5**). Hydrogenation on 30 nm and 50 nm conditions conducts to $i-V_{oc}$ around 720 mV and carrier lifetime values greater than 4 ms. Compared to the reference process integrating 15 nm poly-Si layers without hydrogenation, this $i-V_{oc}$ value represents a +30 mV improvement for our TOPCon² device.

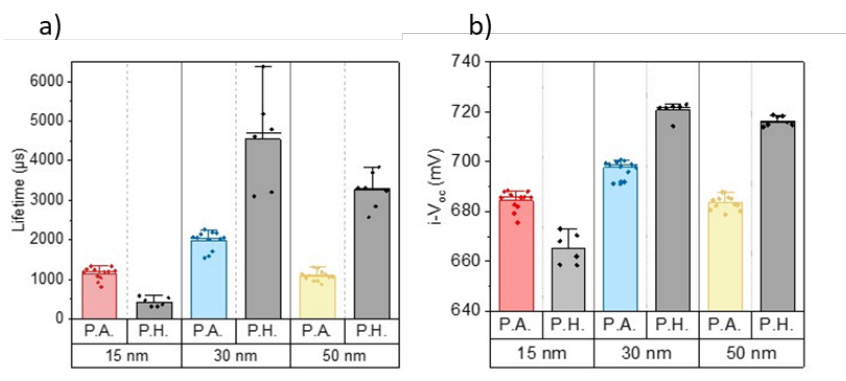


Figure 6: Comparison of a) carrier lifetime values and b) $i-V_{oc}$ for asymmetrical cells precursors after the activation annealing (P.A.) and after the hydrogenation process through SiN:H deposition and removal (P.H.). Data were extracted at an injection level $\Delta n \approx 1E15 \text{ cm}^{-3}$.

3.3 Cell results: toward a tandem application

Complete solar cells were produced from asymmetrical cell precursors. At this stage, only samples without the SiN:H hydrogenation process were brought to cell level. IV characterizations under an AM1.5G spectrum (1 Sun) and a truncated AM1.5G spectrum (IR) were performed. **Figure 7.a** presents the Photovoltaic Conversion Efficiency (PCE) values. The best performance was observed on the 30 nm condition for both illuminations, in good agreement with the passivation data (i.e., $i-V_{oc}$ values).

Looking at V_{oc} (**Figure 7.b**), the 30 nm poly-Si condition, which was exhibiting the best performance on $i-V_{oc}$, also gives the best performance at cell level. Under AM1.5G (1 Sun), a V_{oc} value around 703 mV was obtained with the 30 nm poly-Si condition, corresponding to an improvement of +20 mV compared to the reference process with 15 nm poly-Si layers. Switching to the truncated spectrum (IR), we can see a decrease of around -20 mV for all thickness conditions. The improvement due to thicker poly-Si layers allow the 30 nm condition to exhibit a V_{oc} of around 680 mV under IR spectrum which is as good as the value obtained with the reference process under AM1.5G illumination.

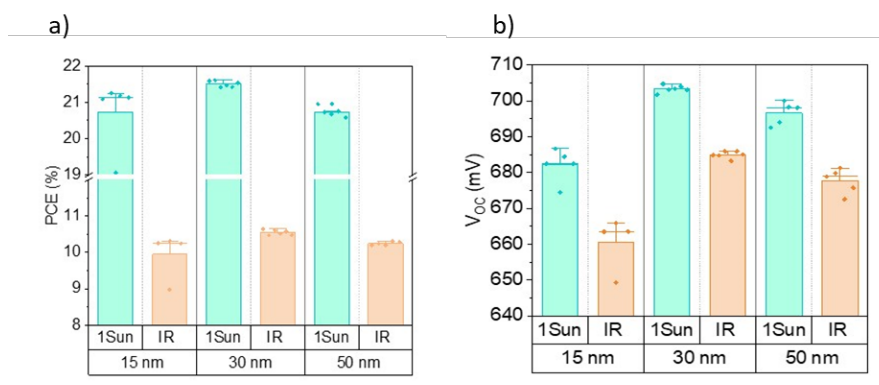


Figure 7: Comparison of a) the PCE and b) the V_{oc} of the fabricated solar cells extracted from IV measurements under AM1.5G (1 Sun) illumination and truncated AM1.5G spectrum (IR).

Focusing now on the Short-Circuit current density (J_{sc}) values (**Figure 8.a**), under AM1.5G illumination we observe that increasing the poly-Si thickness leads to a decrease in J_{sc} values. This decrease is certainly due to a higher parasitic absorption in the poly-Si layers. The J_{sc} values vary from $39.2 \text{ mA}\cdot\text{cm}^{-2}$ to $37.8 \text{ mA}\cdot\text{cm}^{-2}$ when increasing the poly-Si thickness from 15 nm to 50 nm. Such a value might be a limitation for single-junction applications as other technologies can allow better optical response.

However, when analyzing results under truncated spectrum we observe a less pronounced difference for J_{sc} values. When moving from 15 nm thick poly-Si layers to 50 nm, a variation of J_{sc} from $19.7 \text{ mA}\cdot\text{cm}^{-2}$ to $19.5 \text{ mA}\cdot\text{cm}^{-2}$ is observed. This observation shows that the impact of poly-Si parasitic absorption is less significant regarding the wavelengths of interest ($>700 \text{ nm}$) for bottom-cell applications. In addition, a compromise can also be found with the 30 nm condition which even exhibits better V_{oc} performances. This result emphasizes the fact that for tandem applications, an optimization of our TOPCon² toward thicker poly-Si layers is beneficial from a passivation perspective without introducing significant optical limitations due to parasitic absorption. Moreover, the upcoming integration of hydrogenated conditions should allow us to reach higher passivation levels without any other losses.

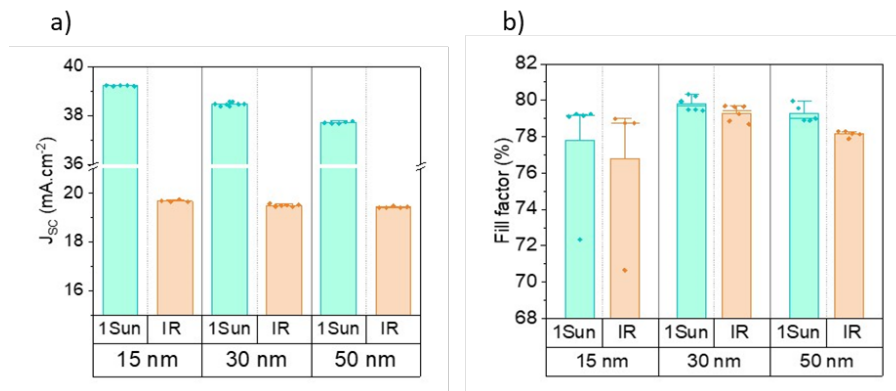


Figure 8: Comparison of a) the J_{sc} and b) the FF of the fabricated solar cells extracted from IV measurements under AM1.5G (1 Sun) illumination and truncated AM1.5G illumination (IR).

We also analyzed the Fill Factor (FF) performances (**Figure 8.b**). Regarding the AM1.5G spectrum, if the FF was slightly better for the 30 nm thickness condition, for all the samples, the FF values were around 79%-80% with a greater dispersion for the 15 nm conditions. When switching to the IR spectrum, we observed a decrease of the FF values, between 1-2%_{abs.} for all the samples.

In order to get a better understanding of the parasitic resistances in our devices, we then analyzed the series resistances (R_s) and shunt resistances (R_{sh}) extracted from illuminated I-V data. **Figure 9** shows the R_s and R_{sh} values for all thickness conditions under AM1.5G (1 Sun) illumination and the filtered AM1.5G spectrum (IR illumination).

Regarding R_s results (**Figure 9.a**), under AM1.5G spectrum, we can see that all splits ultimately present low R_s ($< 0.6 \Omega\cdot\text{cm}^2$). However, we note that the 30 nm-thick poly-Si condition presents the lowest R_s with values below $0.4 \Omega\cdot\text{cm}^2$. The 15 nm-thick poly-Si condition, on the other hand, shows the highest R_s (above $0.45 \Omega\cdot\text{cm}^2$). The 50 nm-thick exhibits a lower R_s than the 15 nm but presents a slightly greater dispersion. The origin of the differences in R_s between the different splits is not clearly identified at this stage. The hypothesis of the impact of metallization must be ruled out, as all cells undergo the same metallization process. When switching to the filtered AM1.5G spectrum (IR), we observe that R_s is decreasing for all the samples but also the differences between the different conditions are then more pronounced. This trend seems to show that R_s is not responsible for the drop in FF observed under the filtered 1 sun spectrum (**Figure 8.b**), since R_s decreases under low illumination.

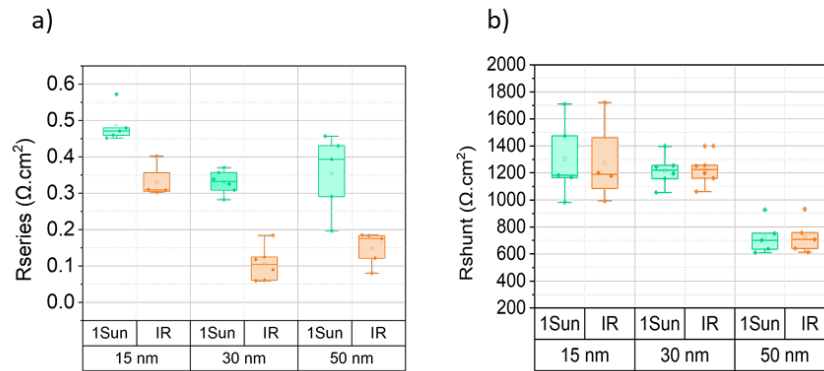


Figure 9: a) R_s and b) R_{sh} values extracted under AM1.5G (1 Sun) illumination (green) and the truncated AM1.5G illumination (orange).

On the other hand, we analyzed the R_{sh} results (**Figure 9.b**). The 50 nm condition features the lower R_{sh} (around $600 \Omega \cdot \text{cm}^2 - 950 \Omega \cdot \text{cm}^2$). The 15 nm and 30 nm conditions feature similar FF values, above $1000 \Omega \cdot \text{cm}^2$, despite here again a slightly greater dispersion for the 15 nm condition. We notice that here no difference were observed on R_{sh} when switching to the filtered spectrum (IR). We note that our sample, regardless of thickness condition, exhibit low R_{sh} values ($< 2000 \Omega \cdot \text{cm}^2$). Such values can have a negative impact on FF at low illumination[12]. It is therefore likely that the shunt resistance is responsible for the drop in FF when switching to IR illumination observed in **Figure 8.b**. This hypothesis would be all the more true as the difference in FF seems slightly more marked on the 50 nm-thick poly-Si condition, which also has the lowest R_{sh} .

4. Conclusion

In this work we identified an optimal poly-Si thickness-dopant activation temperature couple allowing significant improvements of the photovoltaic performances of our TOPCon² devices. More precisely, by increasing the poly-Si thickness from 15 nm (reference) to 30 nm and using a dopant activation temperature of 875°C , a gain in $i-V_{oc}$ of 13 mV was obtained on cell precursors (without hydrogenation). We showed that the increase of the poly-Si thickness limited the dopant diffusion within the silicon substrate. We also demonstrated that the samples featuring thicker poly-Si layers positively reacted to subsequent hydrogenation steps, which was not the case of the reference samples with 15 nm-thick poly-Si layers. For cell precursors, this resulted in a gain in $i-V_{oc}$ of 30 mV in comparison with the reference process. By fabricating complete (i.e., metallized) solar cells, we confirmed that increasing the thickness of the poly-Si layers leads to an increase in parasitic absorption and therefore in a drop in J_{sc} values. This drop, which is significant under AM1.5G (1 Sun) illumination, is significantly reduced under truncated AM1.5G spectrum (IR). Interestingly, the cells with the 30 nm-thick poly-Si layers were also among the best in terms of R_s and R_{sh} resistances. Thus, our bottom-cell device can benefit from increased V_{oc} and FF by increasing the thickness of its poly-Si layers, without suffering significant optical limitations. At this stage, the overall device still needs to be further optimized and the next step will concern the fabrication of complete cells with the integration of the hydrogenation step.

Author contributions

Conceptualization, J.D. and T.D.; Investigation, J.D. and T.D.; writing—original draft, J.D.; writing—review and editing, J.D., T.D., A.K. and S.D.; supervision, A.K. and S.D. All authors have read and agreed to the published version of the manuscript.

Data availability statement

The data that support the findings of this study are available from the corresponding author, J.D., upon reasonable request.

Competing interests

The authors declare that they have no competing interests.

Acknowledgement

The authors would like to extend their appreciation to the French Environment and Energy Management Agency (ADEME) for co-funding Julci Ditsougou thesis's work.

References

- [1] M. Boccard et C. Ballif, « Influence of the Subcell Properties on the Fill Factor of Two-Terminal Perovskite–Silicon Tandem Solar Cells », *ACS Energy Lett.*, vol. 5, n° 4, p. 1077-1082, avr. 2020, doi: 10.1021/acsenenergylett.0c00156.
- [2] W. Chi, S. K. Banerjee, K. G. D. I. Jayawardena, S. R. P. Silva, et S. I. Seok, « Perovskite/Silicon Tandem Solar Cells: Choice of Bottom Devices and Recombination Layers », *ACS Energy Lett.*, vol. 8, n° 3, p. 1535-1550, mars 2023, doi: 10.1021/acsenenergylett.2c02725.
- [3] S. W. Glunz *et al.*, « Silicon-based passivating contacts: The TOPCon route », *Progress in Photovoltaics*, vol. 31, n° 4, p. 341-359, avr. 2023, doi: 10.1002/pip.3522.
- [4] F.-J. Haug *et al.*, « Passivating Polysilicon Recombination Junctions for Crystalline Silicon Solar Cells », *Physica Rapid Research Ltrs*, vol. 15, n° 9, p. 2100272, sept. 2021, doi: 10.1002/pssr.202100272.
- [5] B. Marteau, T. Desrues, Q. Rafhay, A. Kaminski, et S. Dubois, « Passivating Silicon Tunnel Diode for Perovskite on Silicon Nip Tandem Solar Cells », *Energies*, vol. 16, n° 11, p. 4346, mai 2023, doi: 10.3390/en16114346.
- [6] C. Oliveau, T. Desrues, A. Lanterne, C. Seron, S. Rousseau, et S. Dubois, « Double-Side Integration of High Temperature Passivated Contacts: Application to Cast-Mono Si », in *2020 47th IEEE Photovoltaic Specialists Conference (PVSC)*, Calgary, AB, Canada: IEEE, juin 2020, p. 1163-1166. doi: 10.1109/PVSC45281.2020.9300752.
- [7] T. Desrues *et al.*, « Poly-Si/SiO_x Passivating Contacts on Both Sides: A Versatile Technology For High Efficiency Solar Cells », in *2021 IEEE 48th Photovoltaic Specialists Conference (PVSC)*, Fort Lauderdale, FL, USA: IEEE, juin 2021, p. 1069-1072. doi: 10.1109/PVSC43889.2021.9518773.
- [8] B. W. H. van de Loo *et al.*, « On the hydrogenation of Poly-Si passivating contacts by Al₂O₃ and SiN thin films », *Solar Energy Materials and Solar Cells*, vol. 215, p. 110592, sept. 2020, doi: 10.1016/j.solmat.2020.110592.
- [9] Z. Rui *et al.*, « On the passivation mechanism of poly-silicon and thin silicon oxide on crystal silicon wafers », *Solar Energy*, vol. 194, p. 18-26, déc. 2019, doi: 10.1016/j.solener.2019.10.064.
- [10] Yuguo Tao *et al.*, « 730 mV implied Voc enabled by tunnel oxide passivated contact with PECVD grown and crystallized n+ polycrystalline Si », in *2015 IEEE 42nd Photovoltaic Specialist Conference (PVSC)*, New Orleans, LA: IEEE, juin 2015, p. 1-5. doi: 10.1109/PVSC.2015.7356218.

- [11] J. Linke *et al.*, « Poly-Si thickness and temperature dependent oxide disruption induced by penetration of the interfacial oxide in (p) poly-Si/SiO_x passivating contacts », *Solar Energy Materials and Solar Cells*, vol. 246, p. 111890, oct. 2022, doi: 10.1016/j.solmat.2022.111890.
- [12] G. Bunea, K. Wilson, Y. Meydbray, M. Campbell, et D. De Ceuster, « Low Light Performance of Mono-Crystalline Silicon Solar Cells », in *2006 IEEE 4th World Conference on Photovoltaic Energy Conference*, Waikoloa, HI: IEEE, 2006, p. 1312-1314. doi: 10.1109/WCPEC.2006.279655.